Hindawi
Advances in Civil Engineering
Volume 2022, Article ID 9101234, 13 pages
https://doi.org/10.1155/2022/9101234

Research Article

A Nonlinear Prediction Model of Antislide Pile Top Displacement Based on MIC-SVR for Jurassic Landslides

Zhiping Huang,[1] Manman Dong ,[2] Xi Du,[3] and Yongping Guan[4]

[1]*School of Civil Engineering & Architecture, Jishou University, Jishou, Hunan, China*
[2]*Department of Engineering Management, Changshu Institute of Technology, Changshu, China*
[3]*School of Environment and Architecture, University of Shanghai for Science and Technology, Shanghai, China*
[4]*Taizhou Transportation Investment Group, Taizhou, China*

Correspondence should be addressed to Manman Dong; manmandong@cslg.edu.cn

Received 20 January 2022; Accepted 7 March 2022; Published 22 March 2022

Academic Editor: Qian Chen

In this study, a nonlinear prediction model of antislide pile top displacement is proposed. Based on the quantitative analysis of the rock mass structure characteristics of the soft and hard interbedded sliding bed in the Jurassic strata, the post-thrust force and geometric characteristics of the top of antislide pile displacement, and bending moment, the main controlling factors affecting the displacement of the top of antislide pile were determined by maximal information coefficient (MIC). Through orthogonal experiment design and 3DEC numerical experiment, a database of main controlling factors (sliding bedrock inclination, thrust size, embedded depth, and pile section size) of pile top displacement was established and a nonlinear prediction model of the displacement of the top of antislide pile based on the main controlling factors was proposed. Finally, two engineering examples were used to validate the performance of this model, with the comparisons of four prediction methods (SVR, MIC-SVR, LSTM, and ELMAN). The results show that the MIC-SVR model has a practical reference value for the prediction of the displacement of the top of an antislide pile in the Jurassic landslide in the Three Gorges Reservoir Area.

1. Introduction

Landslides widely occur in the Three Gorges Reservoir Region in China [1–4]. Antislide piles balance the thrust of the upper sliding body on the sliding surface through the embedded force and passive resistance of the embedded section to stabilize the ground and are widely used to improve the stability of slopes and prevent their excessive movements [3, 5, 6].

In the analysis of antislide piles, the laminated rock structure is usually modeled as an equivalent homogeneous or horizontally stratified body. Martin and Chen [7] examined the effects of spatial variations in soil displacement on the response of piles and pile groups caused by lateral soil movements using a numerical modeling method. Conte et al. [8] conducted a study on the response of reinforced concrete piles under horizontal loading in multilayered soils composed of silty sand and sandy silt. Klar et al. [9] layered the antislide pile and the rock and soil around the pile and then used the numerical results of each layer to study the three-dimensional interaction characteristics between the pile and the foundation rock and soil. Lei et al. [10] studied the response of laterally loaded piles in multilayered elastic soils using a separation-based continuum model. Mylonakis et al. [11] proposed a method for calculating the internal force of a single pile or group of piles in multilayer soil based on the generalized Winkler foundation model. Salgado et al. [12] proposed a semianalytical method for the analysis of pile groups embedded in multilayered elastic soils. Dong et al. [13] studied the mechanical characteristics of stabilizing piles embedded in layered bedrock through numerical tests and model tests. Fattah [14–17] estimated the bearing capacity of open-ended model piles in different conditions, and the end bearing, vertical, and horizontal displacement of

the pile group model were investigated in dry soil under horizontal excitation.

The Three Gorges Reservoir Area is a high incidence area of landslide geological disaster in China, strata of all ages are developed, among which Jurassic strata are the most widely distributed, the number of landslides developed in this stratum accounts for about 67% of the total number of landslides in the whole reservoir area, and the volume accounts for 65% [18]. In the Jurassic strata of the Three Gorges Reservoir Area, there are a large number of sandstone and mudstone interlayers in the rock structure, which is different from the homogeneous rock structure, and shear stress concentration often occurs under the action of gravity, leading to the overall destruction of the weak layer to produce landslides, which needs urgent treatment [13]. The FLAC3D numerical method is used to analyze the influence of the slope angle, thickness similarity ratio, and layer thickness ratio of the sliding bedrock layer on the force and deformation characteristics of the antislide pile [19]. The K method is used to horizontally divide the rock mass foundation coefficient of the sliding bed into n layers, and the displacement of the top of the antislide pile is calculated [20]. The mechanical characteristics of antisliding piles considering the integrated foundation coefficient of sliding beds on composite inclined rock masses are studied.

At present, there are relatively few considerations about the structural surface development of the rock mass in the embedded section. The influence of the structural characteristics of the sliding bedrock mass and the geometric parameters of the antisliding pile should be further studied. Therefore, the influence of the mechanical characteristics of the rock mass and the geometric parameter characteristics of the antislide piles on the internal force and deformation of the antislide piles are analyzed, which has important theoretical significance for the design of antislide piles for Jurassic landslides.

The pile top displacement of antislide piles is an important indicator for monitoring the effect of antislide piles. At present, the displacement of the pile top used for antislide piles is mainly calculated by the combination of theoretical calculations, model tests, and numerical tests, and few machine learning methods are used to study the top displacement of antislide piles. With the development of computer applications, big data mining and machine learning methods have been widely used in geotechnical engineering, especially in landslide displacement prediction. Therefore, it is necessary to develop antislide pile top displacement predictions based on machine learning.

In summary, based on the quantitative analysis of the rock mass structure characteristics of the soft and hard interbedded sliding bed in the Jurassic strata, the post-thrust force and geometric characteristics of the top of antislide pile displacement, and bending moment, the main controlling factors affecting the displacement of the top of antislide pile were determined by maximal information coefficient (MIC). Through orthogonal experimental design and 3DEC numerical experiments, a database of the main controlling factors (sliding bedrock inclination, thrust size, embedded depth, and pile section size) of pile top displacement was established, and a nonlinear prediction model of the displacement of the top of an antislide pile based on the main controlling factors was proposed.

2. Methodology

2.1. Maximal Information Coefficient. The maximal information coefficient (MIC) is a distinct correlation statistic, and MIC measures the association relationship of both linear and nonlinear relationships between input and output variables [21]. The MIC is an excellent data correlation calculation method that has higher accuracy than mutual information (MI).

MIC is aimed at the relationship between two variables that are discretized in a two-dimensional space. The current two-dimensional space is divided into a certain number of intervals in the x and y directions, the scatter points falling in each grid are checked, and the problem of joint probability in mutual information is solved. The calculation formula of MIC is as follows:

$$\begin{aligned} \mathrm{mic}(x;y) &= \max_{a*b<B} \frac{I(x;y)}{\log_2 \min(a,b)}, \\ \mathrm{MIC}[x;y] &= \max_{|X||Y|<B} \frac{I(x;y)}{\log_2(\min(|X|,|Y|))}. \end{aligned} \tag{1}$$

In the formula, a and b are the number of divided grids in the x and y directions, which are essentially grid distributions, and B is a variable. Generally, the size of B is approximately 0.6 of the amount of data.

2.2. Support-Vector Regression. Support-vector regression (SVR) is a nonlinear regression prediction model based on the principle of structural risk minimization, which works by finding the best regression hyperplane in the high-dimensional feature space. The most widely used model is the ε-SVR model based on the insensitive loss function ε, which is determined by the hyperplane [22].

To establish the nonlinear relationship between the displacement of the pile top and the main control factor determined by the MIC, the training samples are mapped into the high-dimensional feature space through a nonlinear mapping function φ, and then, the correlation between the displacement of the pile top and the main control factor is fitted by the regression estimation function $f(x)$ in the high-dimensional feature space, where f(x) is the following:

$$f(x) = W^T \varphi(x) + b, \tag{2}$$

where W^T is the independent variable function coefficient, $\varphi(x)$ is the nonlinear mapping function, and b is the offset.

The ε-insensitive loss function is used to transform the estimated function into a function minimization problem [23].

$$\text{minimize } \frac{1}{2}\mathbf{w}^T\mathbf{w} + C\sum_{i=1}^{i=l}(\xi_i + \xi_i^*),$$
$$\text{subjected to } \begin{cases} \left(\mathbf{w}^T\varphi(\mathbf{F}_i) + b\right) - JRC_i \le \varepsilon + \xi_i \\ JRC_i - \left(\mathbf{w}^T\varphi(\mathbf{F}_i) + b\right) \le \varepsilon + \xi_i^* \\ \xi_i, \xi_i^* \ge 0, i = 1, \ldots, l. \end{cases} \quad (3)$$

In the formula, C is the penalty parameter, which represents the degree of punishment for samples that exceed the error.

Using Lagrangian and optimal conditions, the following dual problem can be obtained [23]:

$$\text{minimize } \frac{1}{2}(\boldsymbol{\alpha} - \boldsymbol{\alpha}^*)^T\mathbf{Q}(\boldsymbol{\alpha} - \boldsymbol{\alpha}^*) + \varepsilon\sum_{i=1}^{i=l}(\alpha_i + \alpha_i^*) + \sum_{i=1}^{i=l}JRC_i(\alpha_i - \alpha_i^*)$$
$$\text{subjected to } \begin{cases} e^T(\boldsymbol{\alpha} - \boldsymbol{\alpha}^*) = 0 \\ 0 \le \alpha_i, \alpha_i^* \le C, i = 1, \ldots, l, \end{cases} \quad (4)$$

among $Q_{ij} = K(\mathbf{F}_i, \mathbf{F}_j)$ $K(\mathbf{F}_i, \mathbf{F}_j) = \phi(\mathbf{F}_i)^T\phi(\mathbf{F}_j)$ where α_i and α_i^* are Lagrangian multipliers; $\mathbf{e} = 1, \ldots, 1^T$ is the unit vector; $\mathbf{Q}$ is a $l \times l$ positive semidefinite matrix; and $K(\mathbf{F}_i, \mathbf{F}_j)$ is the kernel function that transfers the operations in the high-dimensional feature space to the low-dimensional input space through the kernel technique [23]. It should be noted that the commonly used kernel functions include the radial basis function (RBF), sigmoid function, linear function, and polynomial function. The RBF kernel function, which is the most extensive and can effectively deal with nonlinear problems, is used in this study. The model solution of the dual form is as follows [24]:

$$f(\mathbf{F}) = \sum_{i=1}^{i=l}(-\alpha_i + \alpha_i^*)K(\mathbf{F}_i, \mathbf{F}) + b,$$
$$K\left(\mathbf{F}_i, \mathbf{F}_j\right) = e^{-g\left\|F_i - F_j\right\|^2}, \quad (5)$$

where g is the width parameter of the RBF kernel function, which controls the complexity of the SVR solution. The insensitive loss parameter ε, the penalty parameter C, and the RBF kernel function parameter g will greatly affect the generalization ability and prediction accuracy of the SVR model; therefore, the three parameters need to be uniformly optimized.

2.3. Predictive Model Building Steps. Sample databases and actual engineering examples are used as training samples and test samples, respectively. LIBSVM is used to train the model, and the grid search method with a concise algorithm and easy implementation is adopted to optimize the parameter combination (g, ε, and C). The solution obtained by the grid search is the optimal solution in the grid delineation, and the training error caused by random sampling is eliminated through cross validation. Then, the stable and reliable prediction model is obtained.

The main control factor in the training sample is used as the input variable, and the corresponding antislide pile top displacement is used as the target output variable. The support-vector regression model is trained based on the optimal parameter combination obtained by grid search and cross test. By calling the libsvmtrain function of LIBSVM, the support vector x_i, the support-vector coefficient $(-\alpha + \alpha*)$, and the deviation constant D can be obtained, and then, the pile top displacement prediction equation based on the support-vector regression can be obtained. The obtained pile top displacement prediction equation can be used to predict the pile top displacement of antislide piles (see Figure 1).

3. Main Factors of the Top Displacement of the Antislide Pile

3.1. Discrete Element Modeling. To study the influence of each parameter on the deformation of the top of the antisliding pile, a 3DEC discrete element model was established, as shown in Figure 2. The dimensions of the sliding bed are 33 m × 21 m × 30 m. The relevant mechanical parameters are shown in Table 1. To highlight the regularity of the influence of the structural characteristics of the sliding bedrock on the deformation of the pile tops, the following improvements were made to the model. (1) In the model, only the embedded section of the antisliding pile is considered, and the effect of the sliding body on the antislip pile is simplified to a horizontal rectangular uniform load. (2) Due to the small scope of the model and the fact that the antisliding piles are placed in the sliding section where the sliding surface is gently sloping, the sliding surface of the model is assumed to be horizontal. (3) Given that the row monopile can be

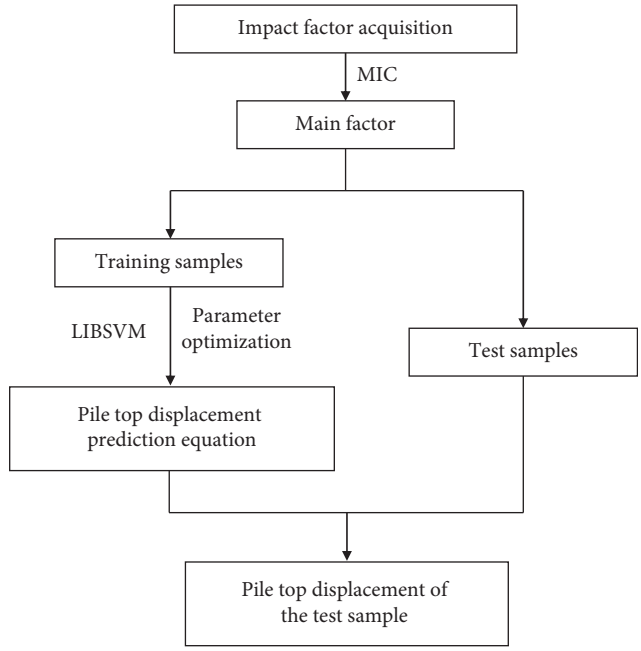

Figure 1: Prediction process of pile top displacement based on MIC-SVR.

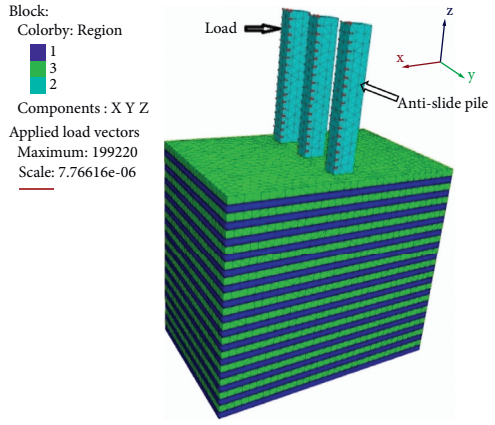

Figure 2: Numerical model.

Table 1: The mechanical parameter of rock.

Category	Bulk modulus (Pa)	Shear modulus (Pa)	Normal stiffness (kPa)	Tangential stiffness (kPa)	Unit weight (kN/m^3)	Cohesion (Pa)	Internal friction angle (°)
Soft rock	1.67×10^9	0.56×10^9	—	—	24.3	2.9×10^5	20
Hard rock	10×10^9	10.9×10^9	—	—	26.5	6.6×10^6	48
Rock layer	—	—	1×10^8	1×10^7	—	0.2×10^6	26
Antislide pile	12×10^9	30×10^9	—	—	30	—	—
Pile rock contact surface	—	—	1.2×10^9	0.1×10^9	—	0.4×10^6	33.8

reduced to a plane strain problem, a total of three antisliding piles are considered, and the intermediate pile is the subject of study [25]. The model is divided before calculation, and the size of mech is 1 m.

Solid element is used to simulate rock, and antislide piles were simulated using solid. The perfect elastic-plastic model (cons = 2) was used for the rock, and the elastic model was adopted to define the behavior of the antislide piles. The

Coulomb sliding failure principal model (jcons = 1) was used for the rock strata. For construction method of the antislide piles, location of the antislide piles is first excavated in the landslide using "tunnel" code, and subsequently, contact surface is used to simulating the interaction of solid element between rock and the antislide piles. Boundary conditions are as follows: normal displacement constraints are applied to the front and rear of the sliding bed, fixed constraints are applied to the bottom boundary, and a horizontal uniform load q in the $-x$ direction is applied to the loaded section of the antisliding pile.

3.2. Influence of Critical Parameters on the Horizontal Displacement of the Antislip Pile

3.2.1. Structural Characteristics of the Soft and Hard Interbedded Layers of Bedrock. To study the influence of the structural characteristics of the soft and hard interbedded layers of bedrock on the displacement of the antisliding pile, the inclination, layer thickness ratio, and single group thickness are selected as the influencing factors for analysis in this study. In the model established in this section, the antisliding pile section size is 2 m × 3 m, the pile length is 30 m, the embedded section is 12 m, and the horizontal load q is 290 kPa.

(1) Inclination of Soft and Hard Interbedded Layers of Bedrock. Since some scholars have pointed out that the influence of the inclination of the counter-inclined rock formation on the antisliding pile is small [19], only the influence of the inclination of the positive-inclined rock formation on the antisliding pile is studied here. The range of rock inclination is 0°~40°, and five parameters are designed as follows: 0°, 10°, 20°, 30°, and 40°. A layer thickness ratio of 1 : 1 (hard rock thickness over soft rock thickness) was used in the model for both hard and soft rocks.

The effect of different inclinations on the displacement of antisliding piles is shown in Figure 3. As seen from the figure, the displacement of antisliding piles corresponding to different inclinations basically show a similar trend with the depth of embedment, while the horizontal displacement of the piles increases with increasing distance from the bottom of the piles and reaches the maximum displacement at the top of the piles. When the inclination angle increases from 0° to 20°, the change in inclination angle has basically no effect on the pile top displacement. When the inclination angle increases from 20° to 40°, the pile top displacement more significantly increases. Compared to an inclination of 0°, the pile top displacement increases by 6.0% and 12.1% for inclination angles of 30° and 40°, respectively, as shown in Figure 4.

(2) Layer Thickness Ratio of Soft and Hard Interbedded Layers of Bedrock. To study the effect of different layer thickness ratios of soft and hard rock on the pile displacement of antisliding piles and considering that the sliding bed of Jurassic stratigraphic landslide in the Three Gorges Reservoir Area is mostly soft and hard interlayer or there are soft and weak interlayers, five groups of layer thickness ratios of soft and hard rock are designed in this paper, namely, 1 : 9, 1 : 7, 1 : 5, 1 : 3, and 1 : 1. The inclination of the soft and hard rock used in the model is 0°, and the thickness of the single group is 2 m.

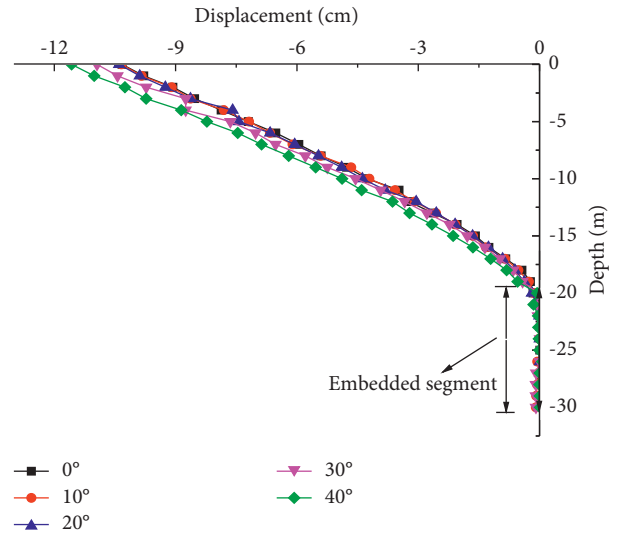

Figure 3: The influence of inclination on the displacement of antislide pile.

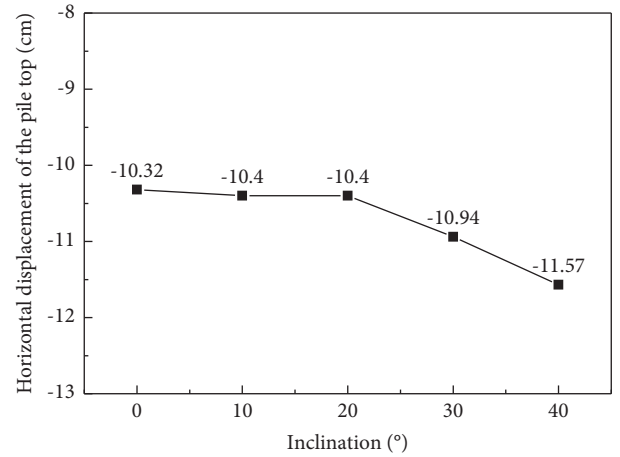

Figure 4: Relationship between the inclination and displacement of the antislide pile.

The effect of different soft and hard rock layer thickness ratios on the displacement of the antisliding pile is shown in Figure 5. As seen from figure, the displacement of the antisliding pile with different rock layer thickness ratios shows a similar trend with the burial depth. In contrast, the horizontal displacement of the pile increases with the distance from the bottom of the pile and reaches the maximum displacement at the top of the pile. With the increase in the layer thickness ratio, the horizontal displacement of the top of the pile shows an increasing linear trend, and the growth is within 3% (see

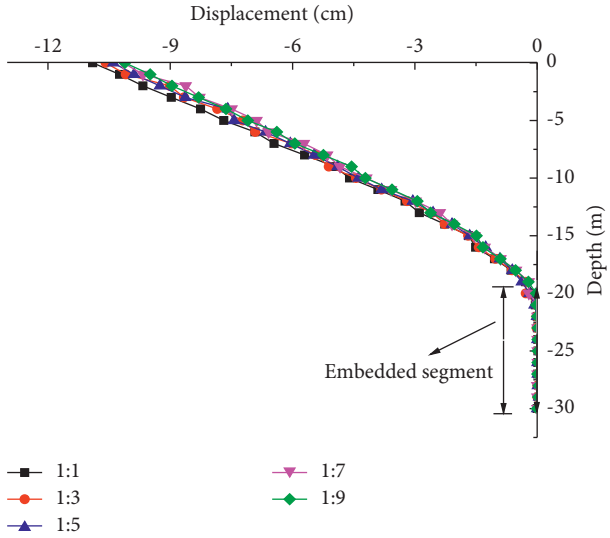

Figure 5: The influence of the layer thickness ratio on the displacement of the antislide pile.

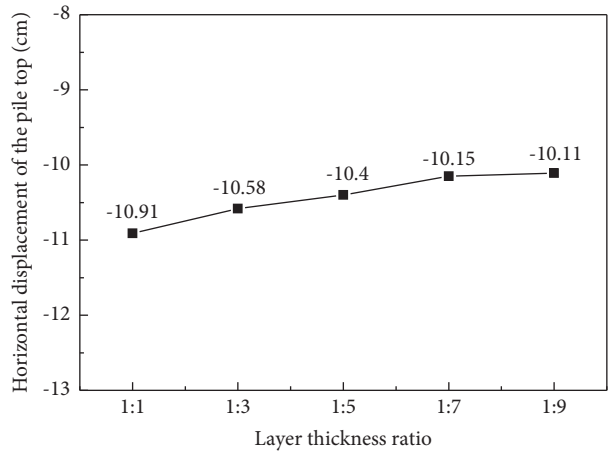

Figure 6: Relationship between the layer thickness ratio and displacement of the antislide pile.

Figure 6). This indicates that the influence of the rock layer thickness ratio on the horizontal displacement of the pile top of the antisliding pile is relatively small.

(3) Thickness of a Single Group of Soft and Hard Interbedded Layers of Bedrock. To study the effect of the single group thickness of soft and hard interlayer rock formations on the displacement of antisliding piles, five groups of soft and hard rock layer thickness ratios are designed in this study, namely,2 m, 4 m, 6m, 8 m, and10 m. The inclination of soft and hard rock used in the model is 0°, and the layer thickness ratio is 1 : 1.

The effect of the thickness of the single group of different rock layers on the displacement of the antisliding pile is shown in Figure 7. As seen from the figure, the displacement of the antisliding pile corresponding to the thickness of a single group of different rock layers shows a similar trend with the depth of burial, with the

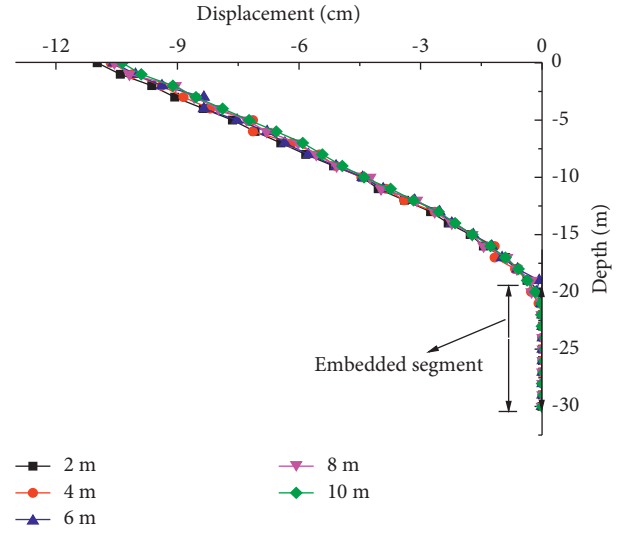

Figure 7: The influence of the single group thickness of rock on the displacement of the antislide pile.

displacement of the top of the antisliding pile being the largest, and the displacement of the pile gradually decreases downward along the top of the pile, tending to zero when it reaches the bottom. When the thickness of the single group of rock layers increases from 2 m to 4 m, the maximum increase in the horizontal displacement of the pile top is approximately 3%, and the rest of the increase in the horizontal displacement of the pile top with the increase in the thickness of the single group is minimal (see Figure 8). This shows that the thickness of a single group of rock layers has a negligible effect on the horizontal displacement of the top of the antisliding pile.

3.2.2. Postpile Thrust of the Antisliding Pile. To study the influence of the postpile thrust on the displacement of the antisliding pile, the influence of the sliding body on the pile is transformed into the magnitude of the postpile thrust to be considered. This study establishes the numerical calculation model of the embedded solid section of an antisliding pile under different thrust conditions, and the postpile thrusts are 1000 kN/m, 1250 kN/m, 1500 kN/m, 1750 kN/m, and 2,000 kN/m. The other parameters in the model are kept consistent in Section 3.2.1.

The effect of different postpile thrusts on the displacement of the antisliding pile is shown in Figure 9. As seen from the figure, the displacement of the antisliding pile corresponding to different postpile thrusts basically shows a similar trend with burial depth, with the displacement of the top of the antisliding pile being the largest, and the displacement of the pile gradually decreases downward along the top of the pile, tending to zero when it reaches the bottom of the pile. The horizontal displacement of the top of the pile shows a gradual increase with the increase in the postpile thrust, when the thrust is between 1250 kN/m and 1750 kN/m, and the horizontal displacement of the top of the pile shows a uniform increase in approximately 20%. When the thrust force is greater than 1750 kN/m, the rate of growth

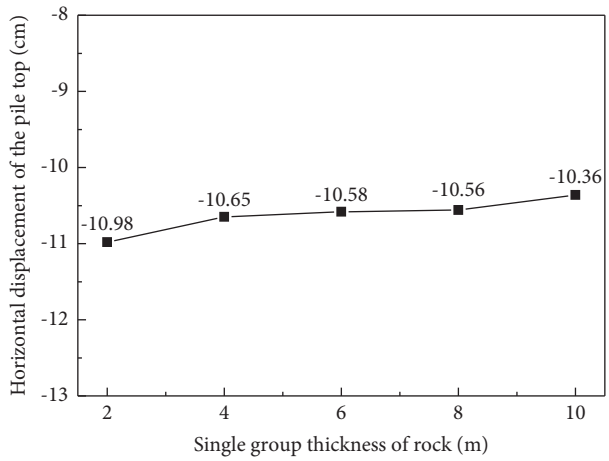

Figure 8: Relationship between the single group thickness of rock and displacement of the antislide pile.

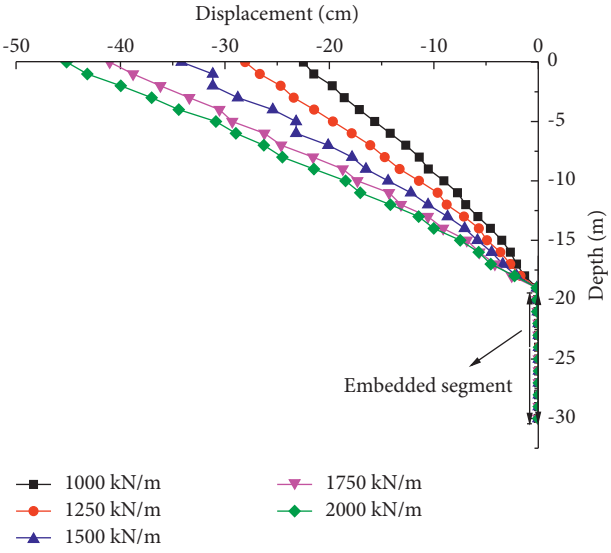

Figure 9: The influence of postpile thrust on the displacement of the antislide pile.

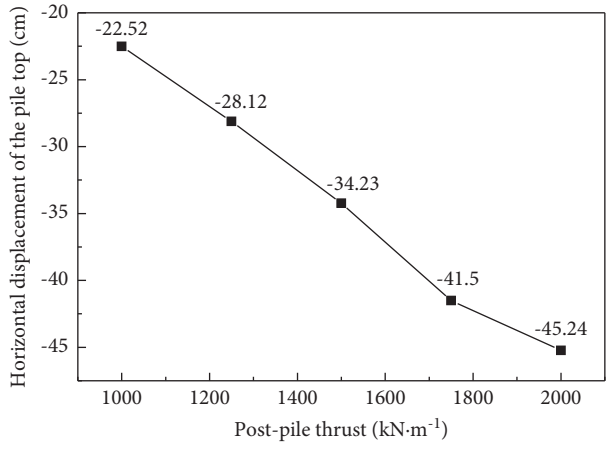

Figure 10: Relationship between postpile thrust and displacement of the antislide pile.

of the horizontal displacement at the top of the pile appears to start slowing down (see Figure 10). This indicates that the magnitude of the postpile thrust has a significant effect on the horizontal displacement of the pile top of the antisliding pile.

3.2.3. Characteristics of the Geometric Parameters of the Antisliding Piles. To study the influence of geometric parameters on the displacement of antisliding piles, the embedded depth and section size are selected as parameters for analysis in this study. In the model established in this section, the inclination of the soft and hard rock used is 0°, the layer thickness ratio is 1 : 1, the thickness of a single group of soft and hard rock layers is 2, and the horizontal load q is 290 kPa.

(1) Depth of Embedded Antisliding Piles. To study the effect of different embedment depths on the displacement of antisliding piles, five sets of embedment depth models are designed in this study, namely, 7 m, 9 m, 11 m, 13 m, and 15 m. The antisliding pile section size is 2 m × 3 m, and the pile length is 30 m.

The effect of different embedment depths on the displacement of antisliding piles is shown in Figure 11. The displacement of antisliding piles corresponding to different embedment depths shows a similar trend with the depth of embedment, with the displacement of the top of the antisliding pile being the largest and the displacement of the pile gradually decreasing downward along the top of the pile and tending to zero when it reaches the bottom of the pile. As shown in Figure 12, when the embedded depth of the antisliding pile increases from 7 m to 9 m, the displacement of the top of the antisliding pile significantly decreases. When the embedded depth of the antisliding pile is greater than 9 m, the change in the displacement of the top of the pile is minimal. Therefore, when designing antisliding piles, it is important to consider not only the stability of the project but also the financial requirements to find a reasonable embedment depth to give sufficient stability to the landslide.

(2) Section Size of the Antisliding Pile. To study the effect of different section sizes on the displacement of antisliding piles, five sets of section sizes were designed in this study, namely, 2 m × 3 m, 2.5 m × 3 m, 2.5 m × 3.5 m, 3 m × 3.5 m, and 3 m × 4 m. In addition, the embedded depth of antisliding piles was 12 m, and the pile length was 30 m.

The effect of different section sizes on the displacement of antisliding piles is shown in Figure 13. As seen from the figure, the displacement of antisliding piles corresponding to different section sizes shows a similar trend with the burial depth, with the displacement of the top of the antisliding pile being the largest, and the displacement of the pile gradually decreasing downward along the top of the pile, tending to zero when it reaches the bottom of the pile. As shown in Figure 14, for section sizes of 2 m × 3 m, 2.5 m × 3 m, 2.5 m × 3.5 m, and 3 m × 3.5 m, changing the antisliding pile section width results in an extremely small trend of change in the displacement of the pile body, while a substantial

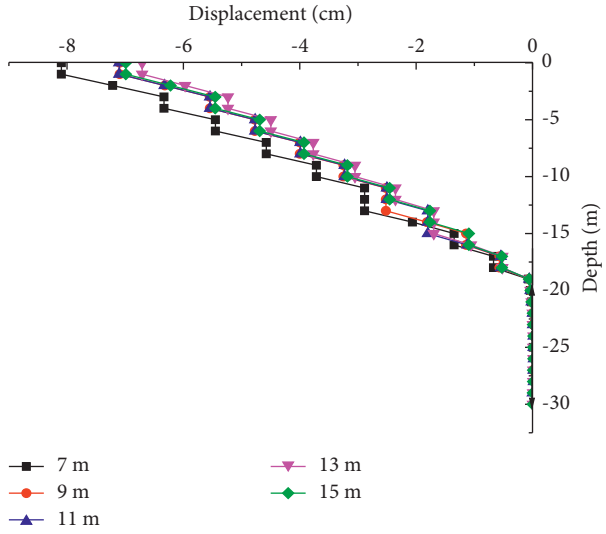

Figure 11: The influence of embedded depth on the displacement of antislide pile.

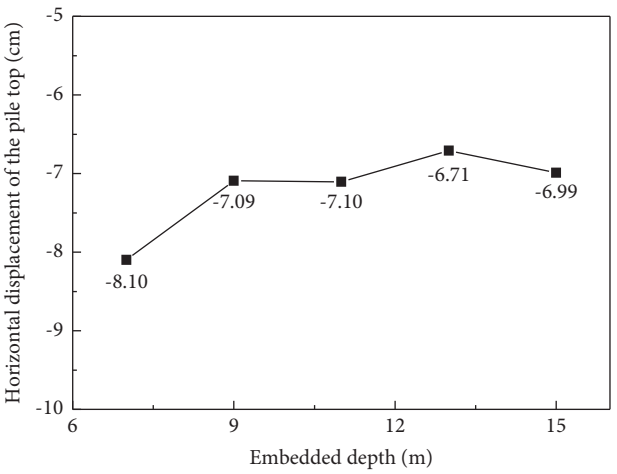

Figure 12: Relationship between embedded depth and displacement of antislide pile.

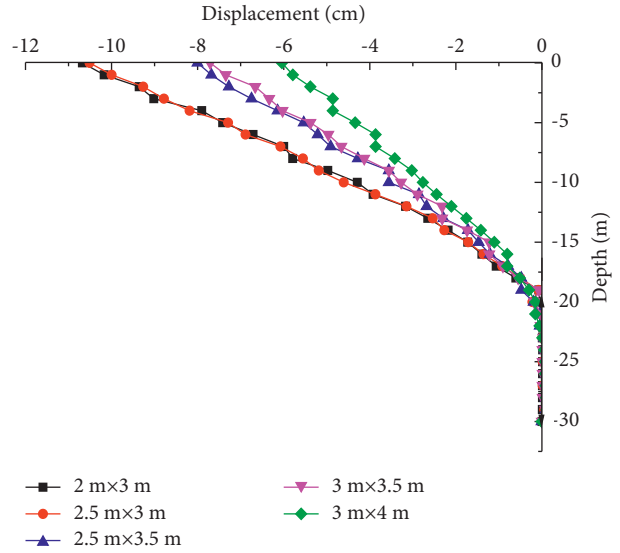

Figure 13: The influence of section size on the displacement of antislide pile.

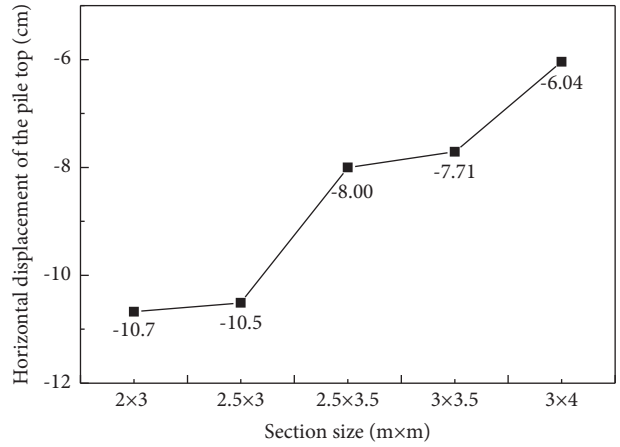

Figure 14: Relationship between section size and displacement of antislide pile.

reduction in the displacement of the top of the antisliding pile occurs when the pile section size is changed from 2.5 m × 3 m to 2.5 m × 3.5 m. The above study results show that the effect of the section length of the antislip pile is greater than the effect of the section width.

3.3. Orthogonal Experimental Design. Orthogonal experimental design is a method to scientifically arrange and analyze multifactor tests using orthogonal tables [26]. With the advantages of ease of use, short cycle time, and good results, orthogonal designs have been widely used in geohazard research [27, 28].

Combined with the results of the above parametric analysis, this test determined six factors: layer thickness ratio of soft and hard rock, the thickness of a single group, the inclination of the slide bed rock, thrust magnitude, embedded depth and pile section size as independent variables, and displacement of the top of the antisliding pile as dependent variables, and carried out a six-factor, five-level orthogonal design, with the factor level table shown in Table 2.

MATLAB software was used to generate orthogonal tables [29] containing a total of 120 sets of tests, and the pile top displacements were calculated using the discrete element numerical simulation software 3DEC. The physical and mechanical parameters and boundary conditions of the model are the same as those of the numerical tests in the previous section. The data from the 120 orthogonal design test results can be considered a sample database regarding the displacements between the pile tops of the soft and hard rock masses of the considered sliding strata and its six independent variables.

3.4. Determination of the Main Control Factor for the Top Displacement of the Antisliding Pile. The MIC values were calculated for the dependent variable (the top displacement of the antisliding pile) and the six influencing factors (rock dip, layer

Table 2: Factor level.

Level	Tested level					
	Inclination (°)	Layer thickness ratio	Single group thickness (m)	Thrust (kN/m)	Embedded depth (m)	Section size (m)
1	0	1 : 1	2	1000	7	2 × 3
2	10	1 : 3	4	1250	9	2.5 × 3
3	20	1 : 5	6	1500	11	2.5 × 3.5
4	30	1 : 7	8	1750	13	3 × 3.5
5	40	1 : 9	10	2000	15	3 × 4

thickness ratio, single group thickness, thrust magnitude, embedment depth, and antisliding pile size), and for the six independent variable influencing factors in relation to each other. The results of the calculations are shown in the table below (see Table 3).

From the MIC values between the antisliding pile top displacement and the six influencing factors, it can be seen that the influences of the antislip pile top displacement are in descending order: postpile thrust > embedded depth > pile section size > rock inclination > single group thickness > layer thickness ratio. The most significant influence on the pile top displacement is the magnitude of the postpile thrust, with the MIC value of the pile top displacement reaching 0.725. Within the sliding bedrock structure feature group, the most influential pile top displacement is the inclination of the soft and hard interbedded rock layers in the sliding bed, suggesting that the inclination of the soft and hard interbedded layers of bedrock contains more information about the variation in pile top displacement. In the group of geometric characteristics of antisliding piles, both the embedded depth and cross-sectional dimensions significantly affect the displacement of the top of the pile, with the MIC values of 0.629 and 0.598, respectively. Therefore, in the case of soft and hard interbedded rock in the sliding bed, the postpile thrust magnitude, pile section size, embedment depth, and rock inclination can be used as the dominant combination of factors to control when predicting the displacement of the top of the antisliding pile.

4. Pile Top Displacement Prediction Model Based on MIC-SVR

4.1. Model Constitution. In this section, four factors, namely, the inclination angle, thrust, embedment depth, and pile cross-sectional size of the soft and hard interlayer of the sliding bed, were used as independent variables, and the displacement of the top of the antisliding pile was used as the dependent variable. A total of 71 sets of experiments were designed on this basis. The discrete element numerical simulation method (3DEC) was used to simulate each set of tests, with the same physical and mechanical parameters and boundary conditions of the model as the numerical tests in the previous chapter. The 71 datasets can be considered as a sample database on the relationship between the pile top displacements and the independent variables considering the soft and hard interbedded layers of bedrock, as shown in Table 4.

4.2. Pile Top Displacement Prediction Model Based on MIC-SVR. Using 71 sets of data as the training database, with the four principal control factors as input variables and their corresponding antisliding pile top displacements as output variables, the optimal combination of parameters $\varepsilon = 0.001$, $C = 0.8745$, and $g = 8.3913$ for the support vector regression was obtained based on grid search and cross validation. Based on the optimal combination of parameters, the optimal SVR model for the prediction of the displacement of the top of the antisliding pile can be obtained. The comparison results between the predicted values of the displacement of the top of the antisliding pile and the numerical test results are shown in Figure 15. The comparison shows that the maximum error between the predicted pile top displacement and the numerical test results is 0.008 m, and most of the errors are small and basically negligible. Therefore, the SVR model obtained through training can well reflect the nonlinear relationship between the antisliding pile top displacement values and the selected primary control factors. The support vector x_i, the support-vector coefficients $(-\alpha, +\alpha\ *)$, and the deviation constant D can be obtained by calling the libsvmtrain function of LIBSVM [30], and 71 support vectors and support-vector coefficients are generated. The value of the deviation constant D is −0.0901. According to equation (6), the prediction equation for pile top displacement based on support-vector regression is obtained as follows:

$$y = \sum_{i=1}^{i=71} \left(-\alpha + \alpha_i^*\right) e^{-8.3913\left\|x_i - x\right\|} - 0.0901. \tag{6}$$

Figure 15 shows a comparison between the predicted and numerical test values of pile top displacement for 71 sets of antisliding piles, with a coefficient of determination R^2 of approximately 96.88% for both sets of data. The results indicate that the accuracy of the established support-vector regression equation is high and is applicable to the prediction of pile top displacement for subsequent examples.

5. Practical Example Validation and Comparative Analysis

5.1. Practical Example Validation. Both the Majiagou No. 1 Landslide and Zhangfeimiao Landslide are located in the Jurassic strata of the Three Gorges Reservoir Area [13, 31], and both landslides use antisliding piles as the support measure. The main control factors and the measured displacement data at the top of the antisliding piles are shown in Table 5.

Equation (6) was used to predict the top displacement of the antislip piles for both landslides. By substituting the inclination, postpile thrust, embedment depth, and pile

Table 3: MIC values between the pile top displacement of the antislide pile and influencing factors.

MIC value	Inclination	Layer thickness ratio	Single group thickness	Postpile thrust	Embedded depth	Section size	Displacement
Inclination	1	0.006	0.006	0.006	0.006	0.003	0.565
Layer thickness ratio	0.006	1	0.012	0.004	0.005	0.001	0.315
Single group thickness	0.006	0.012	1	0.002	0.002	0.002	0.327
Postpile thrust	0.006	0.004	0.002	1	0.005	0.001	0.757
Embedded depth	0.006	0.005	0.002	0.005	1	0.002	0.629
Section size	0.003	0.001	0.002	0.001	0.002	1	0.598
Displacement	0.565	0.315	0.327	0.757	0.629	0.598	1

Table 4: Sample database.

Specimen	Inclination (°)	Postpile thrust (kN/m)	Embedded depth (m)	Section size (m)	Displacement (m)
1	10	1500	15	3 × 3.5	0.124
2	0	1250	11	2.5 × 3.5	0.092
3	20	1250	15	2 × 3	0.126
4	10	1250	13	2 × 3	0.124
5	0	1500	7	2.5 × 3	0.149
6	0	1500	9	3 × 3.5	0.126
7	0	1000	13	2.5 × 3.5	0.077
8	10	1750	7	2 × 3	0.205
9	20	1000	15	2 × 3	0.110
10	10	1750	15	3 × 3.5	0.154
11	40	1500	11	2.5 × 3	0.240
12	0	1000	9	2.5 × 3.5	0.081
13	30	1500	9	2.5 × 3	0.155
14	0	1750	9	3 × 4	0.107
15	10	1250	9	2.5 × 3	0.141
16	10	1750	11	2.5 × 3.5	0.140
17	30	1250	11	2 × 3	0.212
18	0	2000	11	3 × 3.5	0.168
19	0	1000	7	2 × 3	0.112
20	20	1500	11	2.5 × 3.5	0.168
21	20	1250	7	3 × 4	0.118
22	20	1250	7	3 × 3.5	0.130
23	10	2000	7	2.5 × 3.5	0.225
24	10	1000	7	2.5 × 3	0.119
25	20	2000	13	2.5 × 3	0.228
26	30	1750	11	2.5 × 3	0.223
27	30	1250	13	2.5 × 3.5	0.110
28	40	1750	13	2 × 3	0.309
29	40	1250	9	2.5 × 3.5	0.255
30	20	1000	9	2.5 × 3	0.100
31	10	1000	9	3 × 3.5	0.090
32	10	2000	7	2.5 × 3.5	0.225
33	0	2000	11	3 × 3.5	0.157
34	0	1250	13	2.5 × 3	0.116
35	30	2000	9	2 × 3	0.230
36	10	1500	9	3 × 4	0.108
37	10	1750	11	3 × 3.5	0.151
38	40	1000	7	3 × 3.5	0.162
39	30	1750	13	3 × 3.5	0.314
40	10	1000	13	2.5 × 3.5	0.083
41	20	2000	13	2.5 × 3	0.203
42	20	1750	9	2.5 × 3.5	0.180
43	20	1500	7	3 × 3.5	0.163
44	10	1500	13	3 × 4	0.100
45	40	1750	9	2 × 3	0.250
46	0	1250	15	2.5 × 3	0.117

Table 4: Continued.

Specimen	Inclination (°)	Postpile thrust (kN/m)	Embedded depth (m)	Section size (m)	Displacement (m)
47	30	1000	11	3 × 4	0.098
48	40	1000	11	3 × 3.5	0.103
49	20	1500	9	3 × 3.5	0.156
50	0	1500	11	2 × 3	0.134
51	0	1250	13	3 × 3.5	0.096
52	20	1750	13	2.5 × 3.5	0.147
53	30	1000	15	2.5 × 3.5	0.086
54	0	1750	7	3 × 4	0.128
55	40	1250	7	2.5 × 3.5	0.201
56	20	1250	11	3 × 4	0.123
57	30	2000	9	2 × 3	0.233
58	0	1500	13	2 × 3	0.143
59	0	1750	15	2.5 × 3	0.171
60	20	1750	7	2.5 × 3	0.204
61	30	1500	15	2.5 × 3.5	0.140
62	20	1000	13	3 × 3.5	0.085
63	20	1000	9	2 × 3	0.108
64	10	1000	11	2.5 × 3	0.100
65	30	1000	11	2.5 × 3	0.113
66	10	1250	11	2 × 3	0.125
67	30	1250	9	3 × 3.5	0.140
68	30	1000	13	3 × 4	0.070
69	20	1750	11	2 × 3	0.182
70	0	1750	9	2.5 × 3.5	0.141
71	10	1500	13	2 × 3	0.162

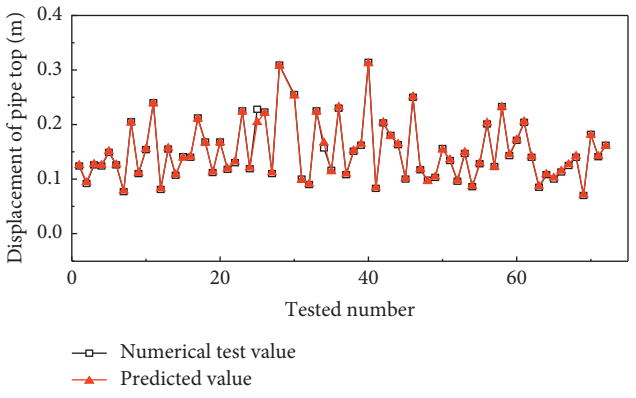

Figure 15: Comparison of the numerical test value and the predicted value.

section size into equation (6) for both landslides, the antisliding pile top displacement y can be calculated to be 0.1447 m and 0.092 m, respectively. The predicted pile top displacement of the Majiagou No. 1 Landslide is approximately 3.5% smaller than the actual value, and the antislip pile top displacement of the Zhangfeimiao Landslide is approximately 8% smaller than the actual value, which indicates that the prediction equation of pile top displacement proposed in this study has good accuracy.

5.2. Comparative Analysis of Predictive Models. To further validate the feasibility of the MIC-SVR prediction model proposed in this study, the prediction results of the Elman neural network, support-vector regression (SVR), and long short-term memory neural network (LSTM) were simultaneously selected in this section for comparison and analysis with the actual values of the two landslides, as shown in Figure 16.

As seen from Figure 16, for the Majiagou No. 1 Landslide, the predictions of the SVR, LSTM, ELMAN, and MIC-SVR models proposed in this study are 14.53 cm, 10.2 cm, 9.3 cm, and 14.47 cm, respectively, and compared to the measured value (15.0 cm), all predictions are small, decreasing by approximately 3.2%, 32%, 38%, and 3.5%. For the Zhangfeimiao Landslide, the predictions of the SVR, LSTM, ELMAN, and MIC-SVR models proposed in this study are 9.3 cm, 7.1 cm, 5.1 cm, and 9.2 cm, respectively, all of which are still smaller than the measured value (10.0 cm), with reductions of approximately 7%, 29%, 49%, and 8%, respectively. For the Zhangfeimiao Landslide, the predictions of the SVR, LSTM, ELMAN, and MIC-SVR models proposed in this study are 9.3 cm, 7.1 cm, 5.1 cm, and 9.2 cm, respectively, all of which are still smaller than the measured value (10.0 cm), with reductions of approximately 7%, 29%, 49%, and 8%, respectively. Combining the comparative prediction results of the two landslides, the SVR model and the MIC-SVR model proposed in this study have higher prediction accuracy, and the results are better than those of the other two prediction models. However, compared with the SVR model, the prediction model proposed in this study, which uses MIC-based screening out the main control factors and circumvents the factors with less influence, not only has a greater advantage in the prediction of pile top displacement of antisliding piles but also reduces the calculation samples and greatly improves the working efficiency. Therefore, the MIC-SVR prediction model proposed

Table 5: The main control factors and the measured value of the antislide pile.

Landslide name	Inclination (°)	Postpile thrust (kN/m)	Embedded depth (m)	Section size (m)	Displacement (m)
Majiagou No. 1	28°	1062.66	8	2 ∗ 3	0.15
Zhangfeimiao	5°	1200	11	2.75 × 3.5	0.10

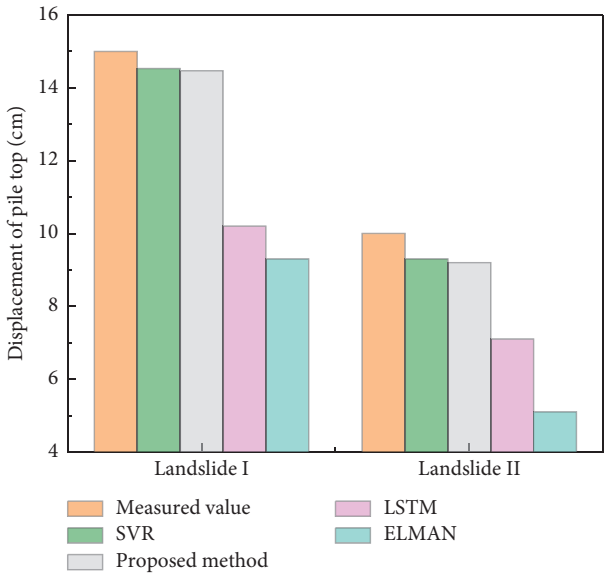

Figure 16: Comparison between the measured value and the predicted value of different methods.

in this study is feasible in practical engineering applications and can better reflect the corresponding relationship between the main influencing factors of the antisliding pile deformation and top displacement of the antisliding pile.

6. Conclusions

(1) The largest influence on the pile top displacement is the magnitude of the postpile thrust, which has an MIC value of 0.725. The most significant influence on the pile top displacement is the inclination of the soft and hard interlayer in the sliding bedrock structure characteristic group. The embedded depth and pile section size of the antisliding pile in the geometry characteristics group greatly influence the pile top displacement, with MIC values of 0.629 and 0.598, respectively. In the case of soft and hard interbedded rock, the postpile thrust, pile section size, embedment depth, and rock inclination are the main control factors in predicting the pile top displacement of the antisliding pile.

(2) A database of pile top displacement concerning the main control factors (sliding bedrock inclination, postpile thrust, embedded depth, and pile section size) was established, and the optimal combination of parameters for SVR was obtained based on grid search and cross validation. On this basis, a nonlinear prediction model of pile top displacement based on the main control factors was developed. The prediction model proposed in this study (MIC-SVR) was compared with SVR, LSTM, and ELMAN by combining practical examples of the Majiagou No. 1 Landslide and Zhangfeimiao Landslide. The prediction model proposed in this study avoids the factors with small influence, reduces the calculation sample, and improves the working efficiency.

Data Availability

The data used to support the findings of this study are included in the article.

Conflicts of Interest

The authors declare that there are no conflicts of interest.

Acknowledgments

This work was supported by the China Postdoctoral Science Foundation Project (grant no: 2016M601338), the Hunan Provincial Department of Education Project (grant no: 18C0562), and the New Faculty Research Initiation Project (grant no: KYZ2021013Q).

References

[1] J. Ma, Y. Wang, X. Niu, S. Jiang, and Z. Liu, "A comparative study of mutual information-based input variable selection strategies for the displacement prediction of seepage-driven landslides using optimized support vector regression," *Stochastic Environmental Research and Risk Assessment*, 2022.

[2] H. H. Zhu, B. Shi, J. F. Yan, J. Zhang, C. C. Zhang, and B. J. Wang, "Fiber Bragg grating-based performance monitoring of a slope model subjected to seepage," *Smart Materials and Structures*, vol. 23, no. 9, pp. 1–12, 2014.

[3] J. Han, D. Liu, Y. Guan et al., "Study on shear behavior and damage constitutive model of tendon-grout interface," *Construction and Building Materials*, vol. 320, Article ID 126223, 2022.

[4] Y. K. Wang, H. M. Tang, J. S. Huang, T. Wen, J. W. Ma, and J. R. Zhang, "A comparative study of different machine learning methods for reservoir landslide displacement prediction," *Engineering Geology*, vol. 298, Article ID 106544, 2022.

[5] L. L. Chen, W. G. Zhang, Y. Zheng, D. M. Gu, and L. Wang, "Stability analysis and design charts for over-dip rock slope against Bi-planar sliding," *Engineering Geology*, vol. 275, Article ID 105732, 2020.

[6] J. W. Ma, X. X. Niu, H. M. Tang, Y. K. Wang, T. Wen, and J. R. Zhang, "Displacement prediction of a complex landslide in the Three Gorges Reservoir Area (China) using a hybrid computational intelligence approach," *Complexity*, vol. 2020, Article ID 2624547, 15 pages, 2020.

[7] G. R. Martin and C. Y. Chen, "Response of piles due to lateral slope movement," *Computers & Structures*, vol. 83, no. 8–9, pp. 588–598, 2005.

[8] E. Conte, A. Troncone, and M. Vena, "Nonlinear three-dimensional analysis of reinforced concrete piles subjected to horizontal loading," *Computers and Geotechnics*, vol. 49, pp. 123–133, 2013.

[9] A. Klar and S. Frydman, "Three-dimensional analysis of lateral pile response using two-dimensional explicit numerical scheme," *Journal of Geotechnical and Geoenvironmental Engineering*, vol. 128, no. 9, pp. 775–784, 2002.

[10] G. Lei, H. Tang, and W. Wu, "A pile-soil separation concerned model for laterally loaded piles in layered soils," *Recent Advances in Modeling Landslides and Debris Flows*, Springer Series in Geomechanics and Geoengineering, Germany, pp. 211–228, 2015.

[11] G. Mylonakis and G. Gazetas, "Settlement and additional internal forces of grouped piles in layered soil," *Géotechnique*, vol. 48, no. 1, pp. 55–72, 1998.

[12] R. Salgado, F. S. Tehrani, and M. Prezzi, "Analysis of laterally loaded pile groups in multilayered elastic soil," *Computers and Geotechnics*, vol. 62, pp. 136–153, 2014.

[13] M. Dong, L. Wang, B. Shahbodagh, X. Du, S. Deng, and Z. Sun, "Effect of the soft and hard interbedded layers of bedrock on the mechanical characteristics of stabilizing piles," *Applied Sciences*, vol. 10, no. 14, p. 4760, 2020.

[14] M. Y. Fattah, H. H. Karim, and M. K. M. Al-Recaby, "Investigation of the end bearing load in pile group model in dry soil under horizontal excitation," *Acta Geotechnica Slovenica*, vol. 18, no. 1, pp. 79–106, 2021.

[15] M. Y. Fattah, H. H. Karim, and M. K. M. Al-Recaby, "Vertical and horizontal displacement of model piles in dry soil with horizontal excitation," *Proceedings of the Institution of Civil Engineers-Structures and Buildings*, vol. 174, no. 4, pp. 239–258, 2021.

[16] M. Y. Fattah, W. H. S. Al-Soudani, and M. Omar, "Estimation of bearing capacity of open-ended model piles in sand," *Arabian Journal of Geosciences*, vol. 9, no. 3, pp. 1–14, 2016.

[17] M. Y. Fattah and W. H. S. Al-Soudani, "Bearing capacity of open-ended pipe piles with restricted soil plug," *Ships and Offshore Structures*, vol. 11, no. 5, pp. 501–516, 2016.

[18] X. X. Liu, Y. Y. Xia, X. S. Zhang, and R. Q. Guo, "Effects of drawdown of reservoir water level on landslide stability," *Chinese Journal of Rock Mechanics and Engineering*, vol. 24, no. 8, p. 6, 2005.

[19] R. Yong, *Interaction between Thrust Load Caused Landslideand Antislide Pile in Jurassic Strata in Three Gorges Reservoir Region*, China University of Geosciences, Wuhan, China, 2014.

[20] H. Z. Zhan, L. Q. Wang, C. S. Wang, and N. Zhang, "Study of mechanical characters of anti-sliding piles considering differentfoundation coefficients of sliding bed [J]," *Rock and Soil Mechanics*, vol. 35, no. S2, pp. 250–256, 2014.

[21] D. N. Reshef, Y. A. Reshef, H. K. Finucane et al., "Detecting novel associations in large data sets," *Science*, vol. 334, no. 6062, pp. 1518–1524, 2011.

[22] P. Samui, "Slope stability analysis: a support vector machine approach," *Environmental Geology*, vol. 56, no. 2, pp. 255–267, 2008.

[23] A. J. Smola and B. Schölkopf, "A tutorial on support vector regression," *Statistics and Computing*, vol. 14, no. 3, pp. 199–222, 2004.

[24] C. S. Wang, *Quatitative Evaluation Methods for Roughness and Peak Shear Strength of Rock Joints*, China University of Geosciences, Wuhan, China, 2019.

[25] The Second Survey and Design Institute of the Ministry of Railways, *Anti-slide Pile Design and Calculation*, China Railway Press, Beijing, China, 1983.

[26] Y. Y. Li, *Experimental Design and Data Processing (Version 2) (M)*, Chemical Industry Press, Beijing, China, 2013.

[27] H. H. Yao, A. X. Wu, Y. M. Wang, and H. C. Xia, "Stability analysis of stope retention pillars in broken rock conditions," *Journal of University of Science and Technology Beijing*, vol. 33, no. 4, p. 400, 2011.

[28] X. Y. Fan, S. J. Tian, and X. D. Duan, "Study of topography factors influence on motion parameters for seismic slope-toe landslides," *ChineseJournalofRockMechanicsandEngineering*, vol. 33, no. s2, p. 4056, 2014.

[29] S. Q. Pang and S. S. Lu, "Construction method of orthogonal table and MATLAB realization," *China Health Statistics*, vol. 34, no. 2, pp. 364–367, 2017.

[30] Z. H. Sun, L. Q. Wang, J. Q. Zhou, and C. Wang, "A new method for determining the hydraulic aperture of rough rock fractures using the support vector regression," *Engineering Geology*, vol. 271, Article ID 105618, 2020.

[31] J. Liu, "Response characteristics of landslide treatment project to reservoir water level change-an example the Zhangfeimiao landslide in the Three Gorges reservoir area," *Yangtze River*, vol. 51, no. 1, pp. 129–135, 2020.